ELSEVIER

Journal of Power Sources 112 (2002) 547–556

JOURNAL OF POWER SOURCES

www.elsevier.com/locate/jpowsour

Properties of mechanically alloyed Mg–Ni–Ti ternary hydrogen storage alloys for Ni-MH batteries

Stéphane Ruggeri[a], Lionel Roué[a,*], Jacques Huot[b], Robert Schulz[b], Luc Aymard[c], Jean-Marie Tarascon[c]

[a]*INRS-Énergie et Matériaux, 1650 Blvd. Lionel-Boulet, C.P. 1200, Varennes, Que., Canada J3X 1S2*
[b]*Institut de Recherche d'Hydro-Québec, 1800 Blvd. Lionel-Boulet, C.P. 1000, Varennes, Que., Canada J3X 1S1*
[c]*Laboratoire de Réactivité et de Chimie des Solides (URA CNRS 1211), Université de Picardie Jules Verne, 33 rue Saint Leu, 80039 Amiens, France*

Received 23 July 2002; accepted 16 August 2002

Abstract

$MgNiTi_x$, $Mg_{1-x}Ti_xNi$ and $MgNi_{1-x}Ti_x$ (with x varying from 0 to 0.5) alloys have been prepared by high energy ball milling and tested as hydrogen storage electrodes. The initial discharge capacities of the Mg–Ni–Ti ternary alloys are inferior to the MgNi electrode capacity. However, an exception is observed with $MgNi_{0.95}Ti_{0.05}$, which has an initial discharge capacity of 575 mAh/g compared to 522 mAh/g for the MgNi electrode. The Mg–Ni-Ti ternary alloys show improved cycle life compared to Mg–Ni binary alloys with the same Mg/Ni atomic ratio. The best cycle life is observed with $Mg_{0.5}Ti_{0.5}Ni$ electrode which retains 75% of initial capacity after 10 cycles in comparison to 39% for MgNi electrodes, in addition to improved high-rate dischargeability (HRD). According to the XPS analysis, the cycle life improvement of the $Mg_{0.5}Ti_{0.5}Ni$ electrode can be related to the formation of TiO_2 which limits $Mg(OH)_2$ formation. The anodic polarization curve of $Mg_{0.5}Ti_{0.5}Ni$ electrode shows that the current related to the active/passive transition is much less important and that the passive region is more extended than for the MgNi electrode but the corrosion of the electrode is still significant. This suggests that the cycle life improvement would be also associated with a decrease of the particle pulverization upon cycling.

Keywords: Hydrogen storage alloys; Magnesium-based compounds; Mechanical alloying; Nickel-metal hydride battery

1. Introduction

Recently, several studies have clearly demonstrated that magnesium-based alloys, particularly nanocrystalline and amorphous Mg–Ni type compounds prepared by mechanical alloying, are promising materials as a metal hydride (MH) electrode for Ni-MH batteries. For example, amorphous MgNi alloy obtained after 10 h of ball milling has an initial discharge capacity of 522 mAh/g [1] in comparison to 280–320 mAh/g for commercial $LaNi_5$-based alloys. In addition, such Mg-based alloys do not need an activation process unlike the conventional AB_5-type and AB_2-type hydrogen storage materials. Lastly, they possess the advantages of very low toxicity and low price (Mg is the sixth most abundant element in the earth's crust). Nevertheless, their charge/discharge kinetics are not yet totally satisfactory and their practical discharge capacities have not attained their theoretical values. Furthermore, the cycle lifetimes of Mg-based electrodes are insufficient from the practical viewpoint. For example, the discharge capacity decay of MgNi electrode is over 70% after only 20 charge–discharge cycles [1]. Such degradation, which nullifies the practical use of magnesium-based alloys as negative electrode materials for Ni-MH batteries, must be drastically reduced. This is a considerable scientific challenge.

The capacity degradation is associated with the irreversible oxidation of the alloy by the electrolyte (KOH) leading to the formation of a $Mg(OH)_2$ layer on the surface of the alloy particles [2–5]. This consumes active material, affects the charge transfer across the alloy/electrolyte interface [4] and may act as a barrier reducing hydrogen diffusion into and from the alloy bulk. Such deleterious phenomena are accentuated by the pulverization of the alloy during charge/discharge cycles which creates new active surface and consequently forms additional $Mg(OH)_2$ after contact with the electrolyte.

A possible way to decrease the capacity loss of Mg-based alloys is to adjust the composition of the Mg–Ni alloys by

* Corresponding author. Tel.: +1-450-929-8185; fax: +1-450-929-8102.
E-mail address: roue@inrs-ener.uquebec.ca (L. Roué).

0378-7753/02/$ – see front matter
PII: S0378-7753(02)00451-2

partial substitution of Mg and/or Ni in order to improve the alloy oxidation resistance in KOH electrolyte and/or to diminish the electrode pulverization by decreasing the alloy expansion coefficient following hydrogen absorption. The partial substitution of Mg and/or Ni may have also an effect on the charge/discharge capacity and kinetics of the electrode by modifying the metal–hydrogen interaction (electronic effect), by modifying the hydrogen-site size (geometric effect) and/or by the formation of additional phases (synergetic effect). Such a partial substitution approach has been successfully used in the case of the commercial AB_5 alloys, which are multicomponent systems derived from $LaNi_5$ alloy with a composition such as (La, Ce, Nd, Pr)(Ni–Co–Mn–Al)$_5$, where the various substitutions for La and Ni have greatly improved the electrode cycle lifetime.

In the last few years, several research groups have conducted studies on the effect of partial substitution on the electrode performance of Mg–Ni-based hydrogen storage alloys. The choice of the substituting elements (nature and number), the substitution ratio as well as the substituted element (Mg and/or Ni) leads to an infinite number of possible combinations. However and in spite of some contradictory studies, a few elements can be identified as promising for the partial substitution of Mg and/or Ni such as:

(i) Cobalt: Ovshinsky's works [6,7] indicate the beneficial effect of Co on the cycle life of Mg–Ni-based electrodes.
(ii) Vanadium: The improvement in cycle life of MgNi alloy by partial substitution of Mg with V is observed because of the preferential oxidization of V or the formation of V oxide layer which reduces the rate of the formation of $Mg(OH)_2$ on the alloy surface during the charge–discharge cycling [8,9].
(iii) Aluminum: Kohno and Kanda demonstrated that it is possible to improve the cycle life of the electrode by using $Mg_{1.9}Al_{0.1}Ni$ rather than Mg_2Ni [10].
(iv) Yttrium: The partial substitution of Mg with Y enhances the resistance of the alloy against corrosion in alkaline media and increases the cycle life of the alloy [11].
(v) Titanium: In the last 2 years, some works indicate that Ti is effective as a partial substitute for Mg from MgNi and Mg_2Ni alloys in improving their cycle life [12–17]. Up to now, the best result was obtained for amorphous $Mg_{0.7}Ti_{0.3}Ni$ alloy, which retains 92% of its initial discharge capacity of 325 mAh/g after 20 cycles [13]. For the same alloy composition and using similar charge/discharge conditions, Zhang et al. obtained an initial discharge capacity of 399 mAh/g and charge retention of 74% after 20 cycles [15]. The cycle life improvement through the partial replacement of Mg with Ti may be associated with the formation of a dense and protective titanium oxide on the alloy surface that suppresses further oxidation of Mg and induces a Ni enriched layer on the alloy surface [13]. In addition, a Mg_2Ni plus TiNi composite material synthesized from elemental Mg, Ni and Ti powders by mechanical alloying shows a charge retention after 150 cycles of 55% while the retention for Mg_2Ni is less than 10% [18].

Among the previous list of substitution elements, titanium appears clearly as a key element for improving the cycle life of Mg–Ni type hydrogen storage electrodes for Ni-MH batteries. The present work provides more extensive data about the influence of Ti on the characteristics of MgNi alloy used as negative electrode in Ni-MH batteries. For that purpose, Ti addition, partial substitution of Mg with Ti and partial substitution of Ni with Ti have been studied through the compared analysis of $MgNiTi_x$, $Mg_{1-x}Ti_xNi$, $MgNi_{1-x}Ti_x$ (with x varying from 0 to 0.5) prepared by high energy ball milling and tested as hydrogen storage electrodes. The results are discussed on the basis of the electrode performance, structure, morphology and surface composition of the materials.

2. Experimental details

2.1. Preparation of the alloys

Pure Mg (99.9%, chips), Ni (99.9%, 325 mesh) and Ti (99.9%, 325 mesh) were used as starting materials. Samples were prepared according to the following stoichiometries: $MgNiTi_x$, $Mg_{1-x}Ti_xNi$, $MgNi_{1-x}Ti_x$ (with $x = 0.05$, 0.2, and 0.5), MgNi, Mg_2Ni, $MgNi_2$, NiTi, $NiTi_2$ and Ni_3Ti. The desired composition mixture (2.3 g) is introduced in a cylindrical steel container (capacity 55 ml) with two 11 mm and one 14 mm diameter steel balls, corresponding to a ball-to-powder mass ratio of 10:1. The container is sealed with an O-ring under argon atmosphere in a glove box. The ball milling was performed for 10 h using a vibratory type mill (SPEX 8000 Mixer). Previous studies indicated that, in such ball milling conditions, contamination of the samples by oxygen, nitrogen or iron atoms through the air introduction and the erosion of the container and balls is very limited (typically, less than 1.0, 0.1 and 0.2 wt.% for O, N and Fe, respectively) [19].

2.2. Characterization

X-ray diffraction (XRD) was performed on a Bruker D8 diffractometer with Cu Kα radiation. Scanning electron microscopy (SEM) observations were made using a Jeol JSM-6300F microscope. X-ray photoelectron spectroscopy (XPS) measurements were performed with a VG Escalab 220I-XL equipped with an Al Kα monochromatic source. The C 1s peak of the adsorbed carbon at 284.6 eV was used as an internal reference to calibrate the peak position. The

atomic surface concentrations were estimated from the Ni 2p, Mg 2p and Ti 2p peaks using a sensitive factor correction. The samples submitted to charge/discharge cycles were rinsed with deionized water and dried overnight at room temperature before XPS and SEM analyses.

The electrochemical charge/discharge cycling tests were performed on an Arbin BT2000 battery tester at room temperature (23 ± 1 °C) in a 6 M KOH solution using a three electrodes cell. The working electrode was a compacted mixture of 100 mg of active material and 800 mg of graphite, plus 20 mg of carbon black. The counter electrode was made of a nickel wire and the reference electrode was an Hg/HgO electrode (XR440 from Radiometer). The electrodes were charged at −200 mA/g for 3 h and discharged at 20 mA/g up to −0.4 V versus Hg/HgO electrode. Polarization curves were carried out at 0.5 mV/s using a Voltalab40 (Radiometer Analytical) potentiostat/galvanostat/FRA apparatus. For these polarization tests, some precautions were taken to avoid any anodic current related to the hydrogen desorption rather than oxides/hydroxides formation, i.e. no cathodic polarization and short immersion period (5 min) in open circuit conditions were done before anodic polarization. The working electrodes used for linear polarization test and for SEM and XPS analysis of cycled materials are constituted of 1 g of pure active material (no carbon added).

3. Results and discussion

3.1. Influence of Ti on the alloy structure

Fig. 1 represents the X-ray diffraction patterns of the Mg–Ni–Ti, Mg–Ni and Ni–Ti alloys. Their phase composition is summarized in Table 1.

Table 1
Structural characteristic of Mg–Ni, Mg–Ni–Ti and Ni–Ti materials

Nominal composition	End product structure[a]
MgNi	a-MgNi
$MgNi_2$	a-$MgNi_2$
Mg_2Ni	n-Mg_2Ni
$MgNiTi_{0.05}$	a-$MgNiTi_{0.05}$
$MgNiTi_{0.2}$	a-$MgNiTi_{0.2}$
$MgNiTi_{0.5}$	a-$MgNiTi_{0.5}$
$Mg_{0.95}Ti_{0.05}Ni$	a-$Mg_{0.95}Ti_{0.05}Ni$
$Mg_{0.8}Ti_{0.2}Ni$	n-Mg_2Ni + n-Ni_3Ti
$Mg_{0.5}Ti_{0.5}Ni$	(a-MgNi + a-NiTi) or a-$Mg_{0.5}Ti_{0.5}Ni$
$MgNi_{0.95}Ti_{0.05}$	a-MgNi + n-Mg_2Ni + n-NiTi + n-Ni
$MgNi_{0.8}Ti_{0.2}$	n-Mg_2Ni + a-NiTi
$MgNi_{0.5}Ti_{0.5}$	n-Mg + n-Ni + n-Ti + a-NiTi
NiTi	a-NiTi
$NiTi_2$	a-$NiTi_2$
Ni_3Ti	n-Ni_3Ti

[a] Nanocrystalline phase (n-); amorphous phase (a-).

As shown in Fig. 1a corresponding to the $MgNiTi_x$ system, a broad peak centered around 42.5° is observed for all compositions implying that Ti addition in MgNi alloy does not modify significantly the amorphization process. For $x = 0.5$, a shoulder is however discernable at ca. 45°, which may reflects the presence of a second phase. These results differ from the study of Han et al. that indicated the formation of a composite alloy made of nanocrystalline Mg_2Ni and TiNi phases for the $MgNiTi_{0.5}$ stoichiometry [18]. One must however note that their milling times were over 15 h, compared to 10 h in the present study. It was previously shown that milling time can have a strong influence on the crystallization process [20].

The XRD patterns of $Mg_{1-x}Ti_xNi$ ($x = 0$, 0.05, 0.2, 0.5) compounds shown in Fig. 1b indicate that all the alloys are amorphous except for $Mg_{0.8}Ti_{0.2}Ni$ composition which is constituted of a mixture of nanocrystalline phases. This is in contradiction with the observations of Zhang et al. [15] and Han et al. [13] where they show the formation of homogeneous amorphous $Mg_{1-x}Ti_xNi$ alloys ($x = 0.1$, 0.2 and 0.3) by mechanical alloying. On the basis of the XRD profiles of various Mg–Ni and Ni–Ti binary alloys obtained using the same milling conditions (see Fig. 1d and e, respectively), one can conclude that, in the present case, the $Mg_{0.8}Ti_{0.2}Ni$ compound contains nanocrystalline Mg_2Ni and Ni_3Ti phases. On the other hand, the mechanically alloyed $Mg_{0.8}Ni$ compound is amorphous (XRD pattern not shown) which tends to confirm that the $Mg_{0.8}Ti_{0.2}Ni$ material is depleted from Ni to form Mg_2Ni phase due to the preferential formation of Ni_3Ti phase. This can be easily explained by the very strong affinity of Ti for Ni in comparison to its affinity for Mg as illustrated by the phase diagrams for the Ni–Ti and Mg–Ti systems [21]. Finally, the preferential reactivity of Ti for Ni illustrated in the case of $Mg_{0.8}Ti_{0.2}Ni$ tends to favor the hypothesis that for $Mg_{0.5}Ti_{0.5}Ni$, the material is constituted by a mixture of a-MgNi and a-NiTi rather than a homogeneous amorphous $Mg_{0.8}Ti_{0.5}Ni$ phase. However, this hypothesis can not be confirmed from XRD analysis because of an overlap between the XRD patterns of a-NiTi and a-MgNi alloys.

Fig. 1c shows XRD profiles of $MgNi_{1-x}Ti_x$ ($x = 0$, 0.05, 0.2, 0.5) materials. The modification of the alloy structure associated with the partial substitution of Ti for Ni is much more marked than for the two previous cases of Ti addition and Mg substitution. For x as low as 0.05, partial crystallization of the alloy is reflected by the appearance of Mg_2Ni phase peaks. On must indicate that, with $MgNi_{1-x}$ compounds, Mg_2Ni phase appeared for $x \geq 0.8$ (results not shown) confirming that Ti atoms accentuates Ni depletion in the Mg–Ni phase through the preferential formation of Ni–Ti phases. For $x = 0.2$, the Mg_2Ni phase becomes more discernable. Lastly, for $x = 0.5$, the XRD pattern shows peaks related to the Mg, Ni and Ti elements which signifies that the alloying process is not yet completed. That is the mechanical alloying kinetic is influenced by the composition of the elemental mixture as observed for the Mg–Ni system

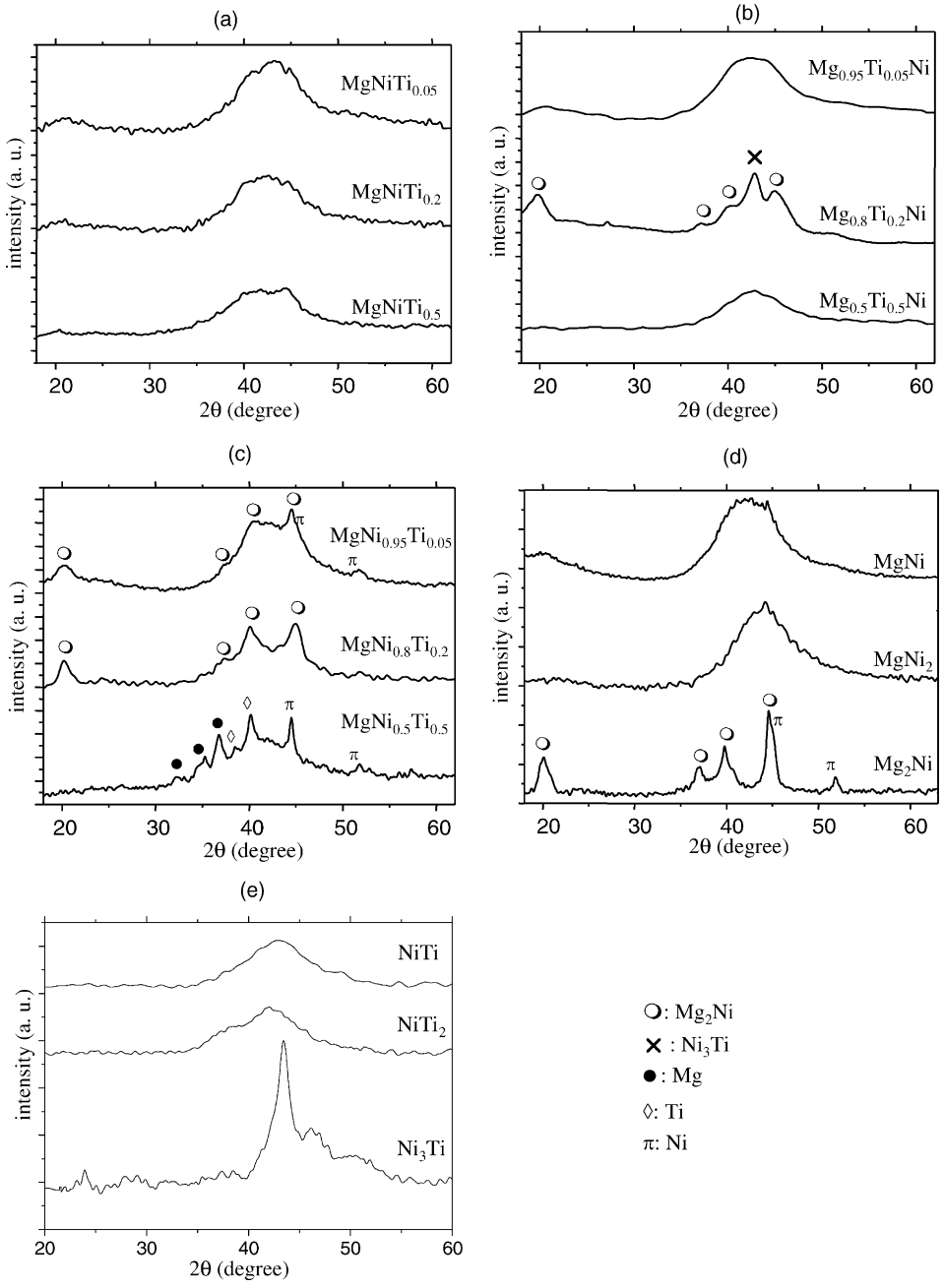

Fig. 1. X-ray diffraction patterns of Mg–Ni–Ti, Mg–Ni and Ni–Ti alloys.

where an increasing Mg/Ni ratio leads to an increasing milling duration for alloying the elemental powders [22].

3.2. Influence of Ti on the cycling dischargeability

The cyclic discharge behavior of the $MgNiTi_x$, $Mg_{1-x}Ti_xNi$, $MgNi_{1-x}Ti_x$, Mg–Ni and Ni–Ti alloys are presented in Fig. 2. Their cycling capacity retention after 10 cycles (C_{10}/C_1) is reported in Table 2.

An important decay in the initial capacity is observed when inactive phases are formed (e.g. Ni_3Ti in $Mg_{0.8}Ti_{0.2}Ni$) and when the compound is not totally alloyed (e.g. $MgNi_{0.5}Ti_{0.5}$). In contrast, a significant increase of the initial discharge capacity is observed for $MgNi_{0.95}Ti_{0.05}$ ($C_1 = 575$ mAh/g) compared to MgNi electrode ($C_1 = 522$ mAh/g). One must note that no increase is measured with homogeneous amorphous $MgNi_{0.95}$ alloy (result not shown). The positive effect on the initial discharge capacity may be associated to the formation of a multiphase structure including a-MgNi major phase, a-NiTi and n-Mg_2Ni minor phases and some Ni inclusions as assumed from structural analysis (see Fig. 1c). This conclusion is supported by several studies reporting an improvement of hydriding/dehydriding properties for various multiphase materials related to the cooperative phenomena

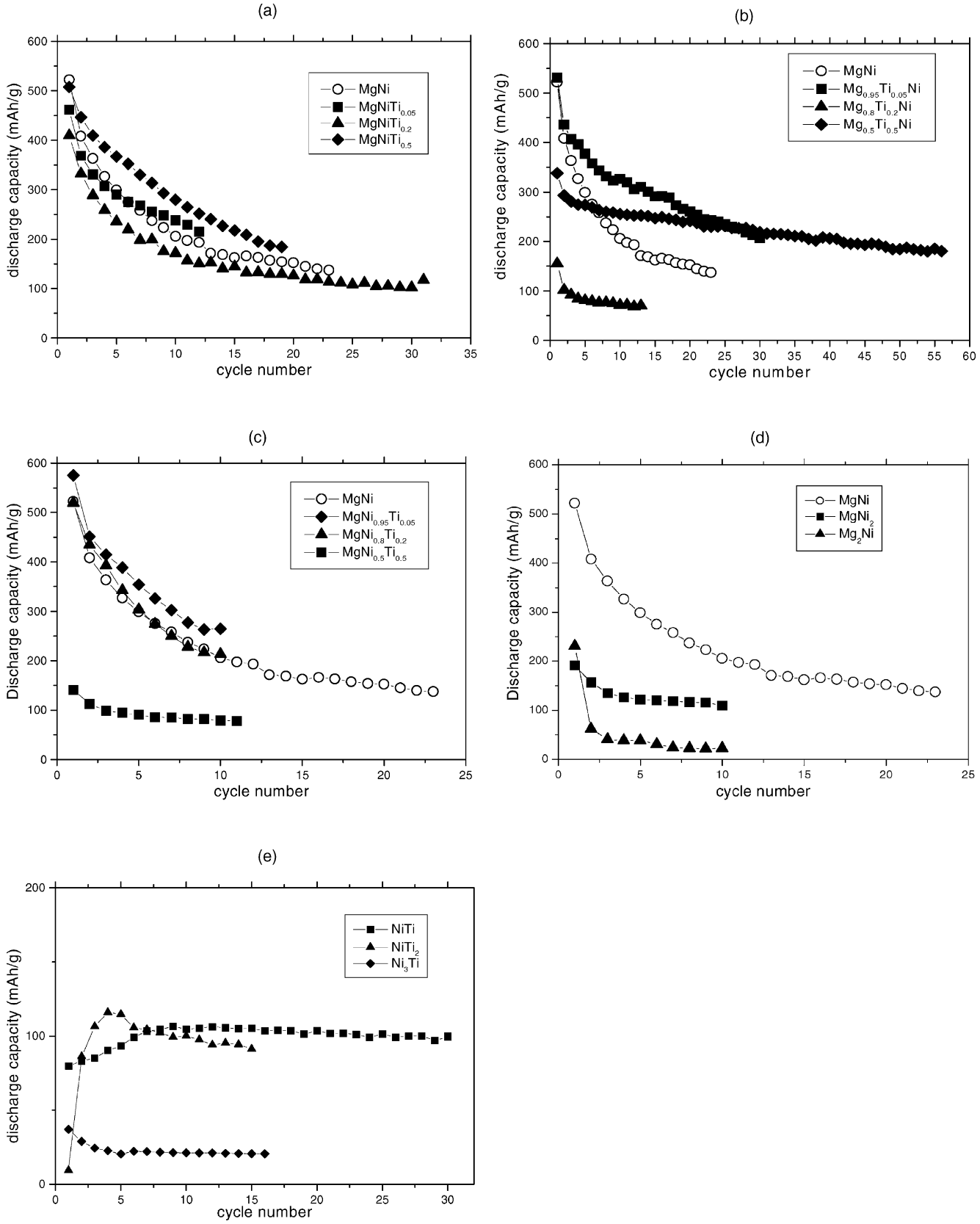

Fig. 2. Cycling discharge capacities of Mg–Ni–Ti, Mg–Ni and Ni–Ti alloys.

Table 2
Cycling dischargeability of the hydrogen storage electrodes

Alloy composition	C_1 (mAh/g)	C_{10} (mAh/g)	C_{10}/C_1 (%)
MgNi	522	206	39
$MgNi_2$	191	110	56
Mg_2Ni	231	23	10
$MgNiTi_{0.05}$	508	280	55
$MgNiTi_{0.2}$	410	172	42
$MgNiTi_{0.5}$	462	238	52
$Mg_{0.95}Ti_{0.05}Ni$	531	327	62
$Mg_{0.8}Ti_{0.2}Ni$	155	71	46
$Mg_{0.5}Ti_{0.5}Ni$	338	255	75
$MgNi_{0.95}Ti_{0.05}$	575	264	46
$MgNi_{0.8}Ti_{0.2}$	519	213	41
$MgNi_{0.5}Ti_{0.5}$	141	79	56
NiTi	80	105	131
$NiTi_2$	9	100	1111
Ni_3Ti	37	21	57

between the different phases constituting nanocomposite hydrogen storage materials [23–31]. The presence of a-MgNi as major phase is however required to achieve high initial electrochemical capacities. In addition, Ni inclusions homogeneously dispersed in the Mg-based material could act as an electrocatalytic site which may reduce the charge transfer resistance during charge/discharge process, resulting in an improvement of the electrode performance as observed in some Mg-based [32], Zr-based [33] and V-based [34] hydrogen storage alloys.

As shown in Table 2, the decrease in discharge capacity retention at 10th cycle is 56% for $MgNi_2$, 39% for MgNi and drops to 10% for Mg_2Ni electrode indicating that the capacity decay of the Mg–Ni-based electrodes proceeds very fast with cycling and is more pronounced with increasing Mg proportion. When Mg–Ni–Ti ternary alloys are compared to Mg–Ni binary alloys with the same Mg/Ni atomic ratio, it appears clearly that Ti is an effective element for improving the electrode cycle life. The best cycle life is observed with $Mg_{0.5}Ti_{0.5}Ni$ electrode which retains 75% of initial capacity after 10 cycles and in less extent with $Mg_{0.95}Ti_{0.05}Ni$ electrode ($C_{10}/C_1 = 62\%$). This confirms recent works indicating that partial substitution of Mg with Ti in Mg-based alloys improves substantially their cycle life [12–17]. The fact that cycle life improvement is not observed for $Mg_{0.8}Ti_{0.2}Ni$ can be explained by the presence in the material of Mg_2Ni phase which is recognized for its very poor cycle life as shown previously (C_{10}/C_1 $Mg_2Ni = 10\%$). Such results emphasize that it is not only the nominal alloy composition but also its structure which changes with the synthesis conditions that must be considered as a key factor to achieve high electrode cycle life improvement. This may explain large differences and even in some cases contradictory results from different authors testing materials with similar nominal composition but having dissimilar microstructure, e.g. homogeneous amorphous $Mg_{0.8}Ti_{0.2}Ni$ alloy has significant improved cycling life ($C_1 \approx 410$ mAh/g, $C_{10}/C_1 \approx 70\%$) [15] in contrast to the present multiphase nanocrystalline $Mg_{0.8}Ti_{0.2}Ni$ material constituted of $Mg_2Ni + Ni_3Ti$ phases ($C_1 = 155$ mAh/g, $C_{10}/C_1 = 46\%$).

3.3. Influence of Ti on the high-rate dischargeability

The initial discharge curves of $Mg_{0.5}Ti_{0.5}Ni$, NiTi and MgNi electrodes are presented in Fig. 3. No evident

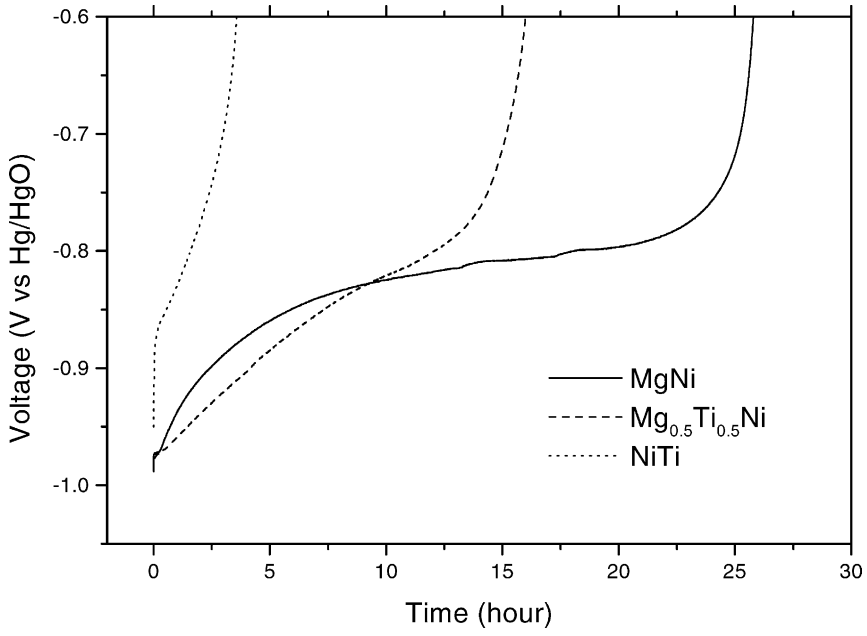

Fig. 3. Discharge curves (first cycle) of MgNi, NiTi and $Mg_{0.5}Ti_{0.5}Ni$ electrodes.

discontinuity characteristic of multiphase hydride appears in the discharge curve of $Mg_{0.5}Ti_{0.5}Ni$. This seems to indicate that $Mg_{0.5}Ti_{0.5}Ni$ material is a mono-phase compound rather than a mixture of MgNi and TiNi phases as expected previously (see structural analysis section). However, the hypothesis of a multiphase system can not be totally rejected because a broadening of the energy spectrum of each type of H occupation site may occur in ball milled composite materials resulting in the disappearance of the discontinuities of the discharge curve [26]. This may be reflected in the steep character of discharge curve of $Mg_{0.5}Ti_{0.5}Ni$ in contrast to MgNi discharge curve where a plateau potential is discernable. This illustrates the large range of hydrogen-site energies for $Mg_{0.5}Ti_{0.5}Ni$ material in comparison to the narrow distribution of energy levels for hydrogen-site in MgNi alloy related to the restricted type of nearest metal coordination as $2Mg_2Ni$ [35]. Additionally, the discharge potential for $Mg_{0.5}Ti_{0.5}Ni$ electrode is more negative than that for MgNi electrode. This can be related to a decrease of the hydride stability or an improvement of the charge-transfer reaction at the surface of the alloy or else to an increase of the hydrogen diffusivity in the material that can have a positive influence on the electrode dischargeability. This is confirmed by the high-rate dischargeability (HRD) measurement denoted by the $C_1^{200\,mA/g}/C_1^{20\,mA/g}$ ratio (see Table 3), in which $C_1^{200\,mA/g}$ and $C_1^{20\,mA/g}$ are the initial discharge capacity measured at the current density of 200 mA/g and 20 mA/g, respectively. From Table 2, one can note that the HRD is improved by Mg substitution with Ti ($C_1^{200\,mA/g}/C_1^{20\,mA/g} = 63\%$ and 40% for $Mg_{0.5}Ti_{0.5}Ni$ and MgNi, respectively) but is still inferior to the HRD

Table 3
High-rate dischargeability of the hydrogen storage electrodes

Alloy composition	$C_1^{20\,mA/g}$ (mAh/g)	$C_1^{200\,mA/g}$ (mAh/g)	$C_1^{200\,mA/g}/C_1^{20\,mA/g}$ (%)
MgNi	522	208	40
$Mg_{0.5}Ti_{0.5}Ni$	338	213	63
$MmNi_{3.6}Co_{0.8}Mn_{0.35}Al_{0.25}$[a]	305	228	75

[a] Activated by 15 charge/discharge cycles.

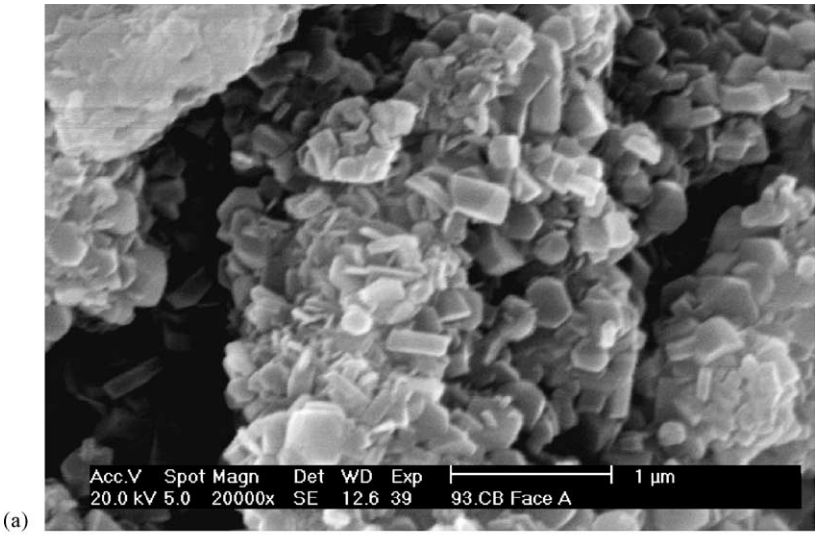

(a)

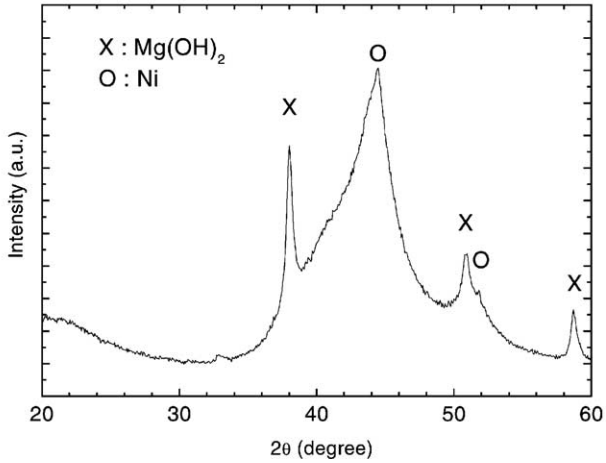

(b)

Fig. 4. (a) SEM image and (b) XRD pattern of MgNi electrode after one charge/discharge cycle.

of commercial $LaNi_5$-based metal hydride ($C^{200\,mA/g}/C^{20\,mA/g} = 75\%$).

3.4. Influence of Ti on electrode corrosion resistance

As shown in Fig. 4a, SEM observation of the MgNi electrode after one charge/discharge cycle reveals the formation of hexagonal platelets characteristic of $Mg(OH)_2$ onto the alloy particles. The appearance of new diffraction peaks on the XRD pattern of cycled MgNi electrode (see Fig. 4b) confirms the partial decomposition of MgNi into $Mg(OH)_2$ and Ni upon cycling. These observations agree with that of other authors [3,5]. In comparison, SEM micrograph of $Mg_{0.5}Ti_{0.5}Ni$ electrode shows after 17 cycles a filamentous structure onto particles (see Fig. 5a). No new phase is clearly discernable from XRD analysis of cycled $Mg_{0.5}Ti_{0.5}Ni$ electrode as shown in Fig. 5b.

XPS analysis was performed before and after cycling in order to identify the filamentous compound formed on $Mg_{0.5}Ti_{0.5}Ni$ particles upon cycle. Our results are listed in Table 4. At first, one must note that the surface composition of the alloy before cycling is far from its nominal composition (i.e. $Mg_{33}Ti_{58}Ni_9$ in comparison to the expected $Mg_{25}Ti_{25}Ni_{50}$ stoichiometry). This may be related to a chemical segregation through the preferential oxidation of Mg and Ti atoms when particles are in contact with air in contrast to Ni atoms which remains in metallic state as established from XPS analysis. After cycling, titanium enrichment onto $Mg_{0.5}Ti_{0.5}Ni$ particles is clearly observable (increase from 58 to 72 at.%). This is accompanied by a decrease of the Mg and Ni surface concentrations from 33 to 22 at.% and from 9 to 6 at.%, respectively. The Ti $2p_{3/2}$ and Ti $2p_{1/2}$ peaks located at 460.1 and 465.8 eV, respectively, are assigned to TiO_2 [36]. The formation of $Ni(OH)_2$ and $Mg(OH)_2$ upon cycling is also established.

As suggested by several authors [13,17], TiO_2 layer formed at the surface of the Mg–Ni–Ti particles may act as a passive film preventing further oxidation of Mg into $Mg(OH)_2$ and consequently, improves the electrode cycle life. In order to confirm this issue, anodic polarization curves for uncharged MgNi and $Mg_{0.5}Ti_{0.5}Ni$ electrodes and for pure Mg powder were performed from open circuit potential to 1.0 V versus Hg/HgO as shown in Fig. 6. For MgNi electrode, a large active/passive transition from −0.87 to 0.5 V versus Hg/HgO followed by a narrow passive region from 0.5 to 0.7 V versus Hg/HgO with a relatively high passive current density of about 14 mA/g. Oxygen evolution is observed from 0.7 V versus Hg/HgO with possible concomitant rupture of the pseudopassive film in connection with the oscillation of the current from 0.8 V versus Hg/HgO. These observations illustrate the low resistance of the MgNi electrode to corrosion in 6 M KOH solution. The

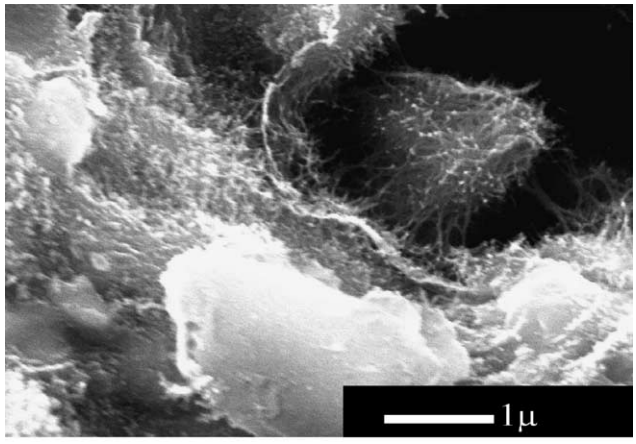

(a)

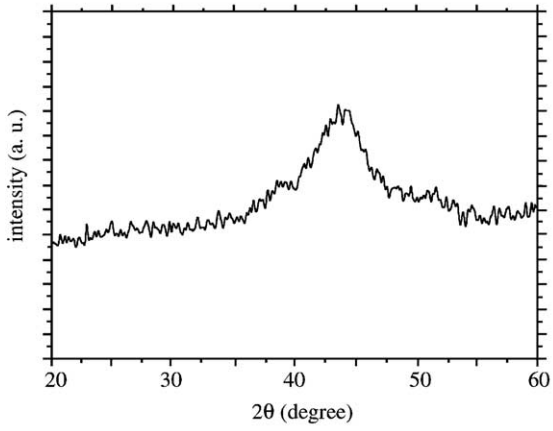

(b)

Fig. 5. (a) SEM image and (b) XRD pattern of $Mg_{0.5}Ti_{0.5}Ni$ electrode after 17 charge/discharge cycles.

Table 4
Surface composition from XPS analysis of $Mg_{0.5}Ti_{0.5}Ni$ electrode before and after 17 charge/discharge cycles

Element/transition	Before cycling		After cycling	
	Peak energy (eV)/assignment	Concentration (at.%)[a]	Peak energy (eV)/assignment	Concentration (at.%)[a]
Mg 2p	49.5 MgO_x	33	49.0 $Mg(OH)_2$	22
Ni $2p_{3/2}$	851.6 Ni	9	857.1 $Ni(OH)_2$	6
Ti $2p_{3/2}$, $2p_{1/2}$	458.0–463.7 TiO or Ti_2O_3	58	460.1–465.8 TiO_2	72

[a] The (Mg + Ni + Ti) concentration is normalized to 1, i.e. oxygen is not considered in the calculation.

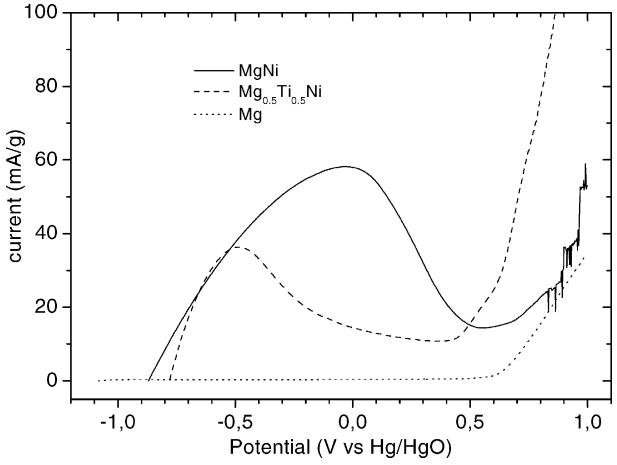

Fig. 6. Anodic polarization curves of MgNi and $Mg_{0.5}Ti_{0.5}Ni$ electrodes in KOH 6 M at scan rate = 0.5 mV/s.

anodic polarization curve of $Mg_{0.5}Ti_{0.5}Ni$ electrode shows that the current related to the active/passive transition is much less important and the passive region is more extended than for MgNi electrode. Furthermore, anodic current is observed from ca. −0.77 V versus Hg/HgO in comparison to −0.87 V for MgNi electrode, reflecting a more noble corrosion potential. Such results confirm the positive influence of Ti on the electrode corrosion resistance. However, one must note that the corrosion of the electrode is still significant in the charge/discharge potential range. This may be associated to the relatively high permeability of the magnesium hydroxide film formed at the surface of the alloy particles. The heterogeneously character of the alloy surface through the presence of Ni and Ti oxide inclusions may prevent the formation of a stable and uniform protective film of $Mg(OH)_2$ observed onto pure Mg powder as illustrated in Fig. 6 where the anodic polarization curve of Mg powder shows an immediate passivation in the anodic region with no active/passive transition and with a passive current as low as 0.3 mA/g.

In other hand, it is well known that metal hydride powder cracks upon cycling due to the expansion and contraction of the lattice cell with hydrogen absorption/desorption process. The fresh alloy/electrolyte interface produced by this way is oxidized promptly with electrolyte and consequently, electrode degradation is accentuated. So, the positive influence of Ti on the $Mg_{0.5}Ti_{0.5}Ni$ electrode cycle life could be also associated with a decrease of the particle pulverization upon cycling. In order to confirm this issue, compared quantification of the electrode pulverization was performed through BET surface area measurements of the MgNi and $Mg_{0.5}Ti_{0.5}Ni$ powders before and after cycling. However, our measurements are altered by the presence of hydroxides/oxides at the surface of the powder after cycling which increases drastically the effective powder surface and consequently, pulverization quantification was impossible. In parallel, hydrogen absorption/desorption cycles were performed in gas phase using a Sievert's apparatus but the high temperature (300 °C) required to desorb hydrogen from the alloys led to their crystallization and consequently, the subsequent BET surface area measurements were also altered. Thus, our investigations did not permit until now to obtain valid quantification of the pulverization of MgNi and $Mg_{0.5}Ti_{0.5}Ni$ electrodes. Additional studies are in progress to clarify this issue by quantifying the alloy expansion followed hydrogen absorption.

4. Conclusions

The electrode characteristics of Mg–Ni–Ti hydrogen storage alloys have been studied with various titanium contents. The major results are summarized as follows:

1. A significant increase of the initial discharge capacity is observed for $MgNi_{0.95}Ti_{0.05}$ ($C_1 = 575$ mAh/g) compared to MgNi electrode ($C_1 = 522$ mAh/g). This positive effect on the initial discharge capacity may be associated with the formation of a multiphase structure.
2. The comparison of the Mg–Ni–Ti ternary alloys to the Mg–Ni binary alloys with the same Mg/Ni atomic ratio shows clearly that Ti is an effective element for improving the electrode cycle life. The alloy structure variation with the ball milling parameters is also a key factor in order to achieve high electrode cycle life improvement. This can explain the contradictory results from materials having similar nominal composition but dissimilar structure.
3. The best compromise between initial discharge capacity and cycle life is observed with $Mg_{0.5}Ti_{0.5}Ni$ electrode where the initial discharge capacity is equal to 338 mAh/g and the capacity retention after 10 cycles is 75% in comparison to 39% for MgNi electrode. In addition, its high-rate dischargeability is improved: $C_1^{200\,mA/g}/C_1^{20\,mA/g}$ equals 63% for $Mg_{0.5}Ti_{0.5}Ni$ in comparison to 40% for MgNi.
4. The cycle life improvement of the $Mg_{0.5}Ti_{0.5}Ni$ electrode seems to be related to the formation of TiO_2 onto the particles which limits $Mg(OH)_2$ formation. However, the corrosion of the electrode is still significant.

Acknowledgements

This work has been financially supported by Hydro-Quebec and the National Sciences and Engineering Research Council of Canada through a Collaborative Research and Development Grant (CRD224841-99) awarded to Prof. L. Roué. The authors also thank to the "Ministère des Relations Internationales du Québec" and the French "Ministère des Affaires Etrangères" for their financial support through a France-Québec grant.

References

[1] S. Ruggeri, C. Lenain, H. Alamdari, G. Liang, J. Huot, R. Schulz, L. Roué, J. Meta. Nanocryst. Mater. 11 (2001) 63–77.
[2] W. Liu, Y. Lei, D. Sun, J. Wu, Q. Wang, J. Power Sources 58 (1996) 243.
[3] N.H. Goo, J.H. Woo, K.S. Lee, J. Alloys Comp. 288 (1999) 286.
[4] T. Abe, T. Tachikawa, Y. Hatano, K. Watanabe, J. Alloys Comp. 330–332 (2002) 792.
[5] C. Lenain, L. Aymard, J.-M. Tarascon, J. Solid State Electrochem. 2 (1998) 285.
[6] S.R. Ovshinsky et al., US patent 5,506,069 (1996).
[7] S.R. Ovshinsky et al., US patent 5,616,832 (1997).
[8] S. Nohara, K. Hamasaki, S.G. Zhang, H. Inoue, C. Iwakura, J. Alloys Comp. 280 (1998) 104.
[9] C. Iwakura, R. Shin-ya, K. Miyanohara, S. Nohara, H. Inoue, Electrochem. Acta 46 (2001) 2781.
[10] T. Kohno, M. Kanda, J. Electrochem. Soc. 144 (1997) 2384.
[11] C. Lenain, L. Aymard, L. Dupont, J.-M. Tarascon, J. Alloys Comp. 292 (1999) 84.
[12] J. Chen, P. Yao, D.H. Bradhurst, S.X. Dou, H.K. Liu, J. Alloys Comp. 293–295 (1999) 675.
[13] S.C. Han, P.S. Lee, J.Y. Lee, A. Zuttel, L. Schlapbach, J. Alloys Comp. 306 (2000) 219.
[14] H. Ye, Y.Q. Lei, L.S. Chen, H. Zhang, J. Alloys Comp. 311 (2000) 194.
[15] Y. Zhang, S.K. Zhang, L.X. Chen, Y.Q. Lei, Q.D. Wang, Inter. J. Hydrogen Energy 26 (2001) 801.
[16] Y. Zhang, B. Liao, L.X. Chen, Y.Q. Lei, Q.D. Wang, J. Alloys Comp. 327 (2001) 195.
[17] C. Iwakura, R. Shin-Ya, K. Miyanohara, S. Nohara, H. Inoue, Electrochem. Acta 46 (2001) 2781.
[18] S.S. Han, N.H. Goo, W.T. Jeong, K.S. Lee, J. Power Sources 92 (2001) 157.
[19] S. Ruggeri, L. Roué, G. Liang, J. Huot, R. Schulz, J. Alloys Comp. 343 (2002) 170.
[20] S. Ruggeri, C. Lenain, L. Roué, G. Liang, J. Huot, R. Schulz, J. Alloys Comp. 339 (2002) 195.
[21] T.B. Massalski, J.L. Murray, L.H. Bennet, H. Baker, L. Kacprzak, Binary Phase Diagrams, vol. 2, ASM, Cleveland, OH, 1991.
[22] S. Ruggeri, unpublished results.
[23] M. Abdellaoui, D. Cracco, A. Percheron-Guegan, J. Alloys Comp. 293–295 (1999) 501.
[24] A. Zaluska, L. Zaluski, J.O. Ström-Olsen, J. Alloys Comp. 289 (1999) 197.
[25] S.I. Orimo, H. Fujii, Intermetallics 6 (1998) 185.
[26] Q.M. Yang, M. Ciureanu, D.H. Ryan, J.O. Ström-Olsen, J. Alloys Comp. 274 (1998) 266.
[27] K.J. Gross, P. Spatz, A. Züttel, L. Schlapach, J. Alloys Comp. 240 (1996) 206.
[28] J. Yang, M. Ciureanu, R. Roberge, J. Alloys Comp. 287 (1999) 251.
[29] H. Nakamura et al., US patent 5,876,869 (1999).
[30] W.K. Choi, T. Tanaka, R. Miyauchi, T. Morikawa, H. Inoue, C. Iwakura, J. Alloys Comp. 299 (2000) 141.
[31] G. Liang, J. Huot, S. Boily, A.V. Neste, R. Schulz, J. Alloys Comp. 297 (2000) 261.
[32] N. Cui, P. He, J.L. Luo, Acta mater. 47 (1999) 3737.
[33] S.R. Ovshinsky, M.A. Fetcenko, Appl. Phys. A 72 (2001) 239.
[34] H. Inoue, R. Miyauchi, R. Shin-Ya, W.K. Choi, C. Iwakura, J. Alloys Comp. 330–332 (2002) 597.
[35] S. Orimo, H. Fujii, Appl. Phys. A 72 (2001) 167.
[36] R.L. Kurtz, V.E. Henrich, Surf. Sci. Spectra 5 (1998) 179.